Konya Mühendislik Bilimleri Dergisi, c. 11, s. 4, 1096-1105, 2023
Konya Journal of Engineering Sciences, v. 11, n. 4, 1096-1105, 2023
ISSN: 2667-8055 (Electronic)
DOI: 10.36306/konjes.1368573

THE EFFECT OF THE AEGEAN SEA EARTHQUAKE, OCCURRED ON OCTOBER 30, 2020, ON TUSAGA STATIONS

[1,*] **Tunahan GUNDOĞAN**, [2] **Sercan BÜLBÜL**, [3] **Cevat İNAL**

[1] *General Directorate of Mapping (GDM), Ankara, TÜRKİYE*
[2,3] *Konya Technical University, Engineering and Natural Sciences Faculty, Geomatics Engineering Department, Konya, TÜRKİYE*
[1] tunahan.gundogan@harita.gov.tr, [2] sbulbul@ktun.edu.tr, [3] cinal@ktun.edu.tr

Highlights

- The effects of The Aagean Sea Earthquake on GNSS measurements
- The effects of GNSS measurements time on point positioning
- The success of GNSS in detecting deformation

***Corresponding Author:** Tunahan GÜNDOĞAN, tunahangundogan7@gmail.com

Konya Mühendislik Bilimleri Dergisi, c. 11, s. 4, 1096-1105, 2023
Konya Journal of Engineering Sciences, v. 11, n. 4, 1096-1105, 2023
ISSN: 2667-8055 (Electronic)
DOI: 10.36306/konjes.1368573

THE EFFECT OF THE AEGEAN SEA EARTHQUAKE, OCCURRED ON OCTOBER 30, 2020, ON TUSAGA STATIONS

[1,*] Tunahan GUNDOĞAN, [2] Sercan BÜLBÜL, [3] Cevat İNAL

[1] *General Directorate of Mapping (GDM), Ankara, TÜRKİYE*
[2,3] *Konya Technical University, Engineering and Natural Sciences Faculty, Geomatics Engineering Department, Konya, TÜRKİYE*
[1] tunahan.gundogan@harita.gov.tr, [2] sbulbul@ktun.edu.tr, [3] cinal@ktun.edu.tr

(Received: 29.09.2023; Accepted in Revised Form: 16.10.2023)

ABSTRACT: GNSS is used to determine the point positions on the earth with high accuracy. The accuracy that can be achieved with GNSS depends on the satellite system, processing software, logging interval, observation time, etc. varies depending on the effects.
In the study, the impact of the Aegean Sea Earthquake that occurred on November 30, 2020, on TUSAGA was investigated. For this purpose, 7 TUSAGA stations located in the earthquake-affected area were selected. The 24-hour RINEX data for these stations were obtained both 15 days before and after the earthquake. The 24-hour RINEX data of 7 TUSAGA were processed using the GAMIT/GLOBK, based on 14 IGS stations. Furthermore, the evaluations were repeated by dividing the 24-hour RINEX data into 2, 4, and 12-hour intervals. In the evaluation, the GPS+GLONASS+Galileo (MIX) satellite configuration was utilized. The daily solutions obtained to reveal the effect of the earthquake are divided into two parts as before/after the earthquake. For each of TUSAGA stations, pre- and post-earthquake coordinates and RMSE were calculated. With statistical tests, whether the changes in the points are significant or not, the amount and direction of the changes were determined with 95% statistical confidence. As a result, it was concluded that the changes before/after the earthquake were mostly in the MNTS, which is the closest to the earthquake base, the changes in the points generally decrease as you move away from the earthquake center, and the evaluation before/after the earthquake can be made more healthy as the observation time increases. In addition, 30-day coordinates were examined through time series, and only the graph of the change in MNTS was given since it was the closest station to the epicenter of the earthquake.

Keywords: *The Aegean Sea Earthquake, Galileo, GLONASS, GPS*

1. INTRODUCTION

According to national and international seismology centers, on October 30, 2020, at 14:51 local time in Turkey, an earthquake with its epicenter in the Aegean Sea, 8 kilometers north of Samos Island and at a depth of 10-12 kilometers occurred. The earthquake's magnitude was reported as Mw: 6.6 according to the Disaster and Emergency Management Authority (AFAD) data and Mw: 6.9 according to the Kandilli Observatory and Earthquake Research Institute (KRDAE). The earthquake was felt in various regions, primarily in İzmir, as well as in Muğla, Aydın, Denizli, Manisa, Uşak, Afyonkarahisar, Kütahya, Balıkesir, Bursa, Çanakkale, Istanbul, and Sakarya provinces, along with all of Western Anatolia and the North Aegean Islands [1].

The region where the October 30, 2020 Aegean Sea earthquake occurred represents a geographical area that includes the southern part of the Greek mainland to the west, the Aegean Sea in the middle, and Western Anatolia to the east. The Aegean Region, extending over approximately 800 kilometers along a North-South direction, experiences deformation under the North-South extension tectonics due to the subduction of the African plate beneath the Eurasian plate [2].

The Aegean Sea Earthquake took place in the central part of the Aegean Region, which is significantly deformed due to the effects of the North-South extension tectonics. This area is characterized by the subduction of the African plate beneath the Eurasian plate, resulting in substantial crustal deformation. It

***Corresponding Author:** Tunahan GÜNDOĞAN, tunahangundogan7@gmail.com

is also a seismogenic zone where intense seismic activity occurred both before and after the year 1900 [1].

Contemporary regional positional changes after earthquakes can be estimated by utilizing continuously monitored GNSS (Global Navigation Satellite System) stations [3]. Numerous studies have been conducted in this regard. In Thailand, following the 2004 earthquake near Banda-Aceh with a magnitude of Mw: 9.3 and the 2005 earthquake near Nias Island in Sumatra with a magnitude of Mw: 8.7, the effects of these earthquakes on the Thai Geodetic GPS Network were investigated using the PPP (Precise Point Positioning) method with GIPSY-OASIS-II software. As of the end of 2006, horizontal movements of up to 55 cm in the south and 6 cm in the north of Thailand were determined [4]. Vertical movements in Houston, a subsidence area for many years, have been attempted to be determined using the CORS network. OPUS, a web-based GNSS evaluation software, and the scientific GNSS evaluation software GIPSY/OASIS were used to evaluate the measurements. Subsidence up to 0.5 cm per year can be detected using the OPUS software with long-term GNSS data of 5 years or more [5]. A method has been developed for real-time and high-precision tracking of earthquakes using a single-frequency GPS receiver. The analysis of the Wenchuan earthquake with a magnitude of Mw: 8.0, the Tohoku-Oki earthquake with a magnitude of Mw: 9.0, and the Lushan earthquake with a magnitude of MW: 6.6 has been performed. The results show that accurate and reliable results can be obtained using the developed method [6]. When analyzing landslides in Alaska through time series of GPS observations spanning 4 years, horizontal movements of 5.5 cm/year in the east-west direction and vertical movements of 2.6 cm/year have been detected in the north [7]. By using measurements from 43 GNSS stations scattered throughout the Southern Patagonian Icefield region, horizontal velocities with an accuracy of approximately 1 mm/year and vertical velocities of about 6 mm/year have been determined, and these velocities were used to determine the shape and magnitude of horizontal and vertical crustal deformation [8]. GPS observations with 30-second recording intervals conducted on July 15-18, 2013, and December 7-10, 2013, were used to investigate the post-seismic movement of the strike-slip fault in Northern Sumatra following the Aceh earthquake with a magnitude of 6.1 that occurred on July 2, 2013. The measurements were evaluated using the Bernese v5.2 software. As a result of the post-seismic deformation analysis of the Aceh earthquake, it was observed that the earthquakes that occurred before, in 2004 and 2012, were still affecting Northern Sumatra, with effects of approximately 12 mm and 10 mm, respectively [9]. Deformations resulting from the earthquake with a magnitude of Mw: 7.9 that occurred on April 25, 2015, in Gorkha have been determined based on measurements made before and after the earthquake using 6 GNSS stations. In the evaluation of the measurements, the Bernese v5.2 software was used, and post-seismic displacement was obtained from daily time series data that had been corrected for interseismic deformation and seasonal changes [10]. It is also known that earthquakes with a seismic moment magnitude of less than Mw 6.0 do not create surface displacements measurable with the global positioning system (GPS) [11]. Studies have shown that increasing the observation duration and using multiple satellite systems together improve positional accuracy [12]. Earthquake monitoring studies with GNSS have been one of the topics of interest in recent years [13]–[18] .

In this context, GNSS receivers at TUSAGA points in the earthquake region were able to record data from GPS, GLONASS, and Galileo satellite systems, so all three satellite systems were used in the study. Daily RINEX data from 7 TUSAGA stations (AKHI, BOZU, CINC, ESME, MNTS, SHUT, and TVAS) were divided into 2, 4, and 12-hour segments, and the solutions were evaluated using the GAMIT/GLOBK data evaluation software with GPS+GLONASS+Galileo (MIX) satellite combination.

2. EXPERIMENTAL DETAILS

On October 30, 2020, a very powerful earthquake occurred in the Aegean Sea, between the north of Samos Island and the Doğanbey-İzmir offshore area (37.9020 North, 26.7942 East) at 14:51 local time, according to AFAD (Disaster and Emergency Management Authority). The earthquake was reported to have a magnitude of Mw=6.6 by AFAD and Mw=6.9 by KRDAE. The depth of the earthquake's focus was approximately 12 kilometers, indicating it was a shallow-focus earthquake. The earthquake was felt in a wide area, including İzmir province and its districts, as well as the Aegean and Marmara regions.

The Turkey Earthquake Hazard Map was updated on January 1, 2019, and came into effect. In this map, instead of earthquake zones, the largest ground acceleration values (PGA: Peak Ground Acceleration) were shown, and the maximum acceleration value for İzmir province was determined to be between 0.3-0.5g (PGA 475_{year}). These values indicate a high earthquake hazard in the region (Figure 1).

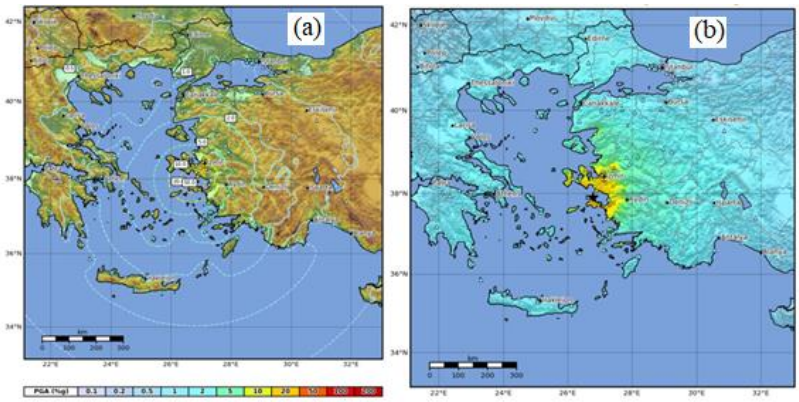

Figure 1. Aegean Sea Earthquake (a) PGA and (b) Intensity Map (https://earthquake.usgs.gov/earthquakes/eventpage/us7000c7y0/shakemap/intensity)

The province of İzmir is located at the western end of the Gediz Graben system, which is under the influence of the Western Anatolian Extensional Regime. As can be seen in the Turkey Active Fault Map prepared by the MTA (General Directorate of Mineral Research and Exploration) in 2011, east-west trending normal faults are situated at the western end of the Gediz Graben, whereas especially northeast-southwest and northwest-southeast trending faults concentrate around the İzmir region. Apart from the Gediz Graben, active faults in the region that could contribute to earthquake activity include the Tuzla, Seferihisar, Gülbahçe, Mordağan, Gümüldür, İzmir, Menemen, Güzelhisar, Yeni Foça, and Kiraz faults (http://www.koeri.boun.edu.tr/sismo/2/wp-content/uploads/2020/10/20201030_izmir_V1.pdf).

To determine the changes in the region affected by the Aegean Sea earthquake on October 30, 2020, GNSS data from 7 TUSAGA points were used (Figure 2).

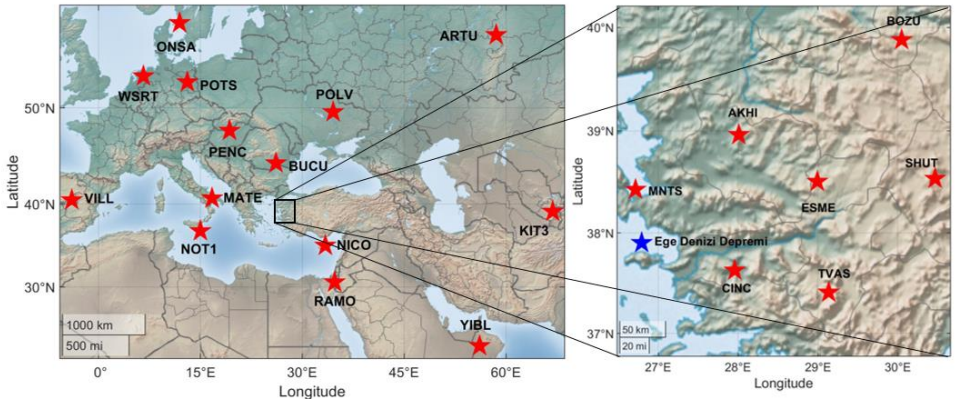

Figure 2. Used IGS (left) and TUSAGA Stations (right)

To investigate the changes in the TUSAGA stations in the earthquake region, RINEX data for 2, 4, and 12-hour intervals were collected using GNSS from the Akhisar (AKHI), Bozüyük (BOZU), Çine(CINC), Eşme (ESME), Menteş (MNTS), Şuhut (SHUT), and Tavas (TVAS) TUSAGA stations. The GAMIT/GLOBK software was used for the MIX solution. In the analysis of the selected TUSAGA stations, the IGS stations ARTU, BUCU, KIT3, MATE, NICO, NOT1, ONSA, PENC, POLV, POTS, RAMO, VILL, WSRT, and YIBL were used as references (Figure 2).

To investigate changes in the TUSAGA stations, RINEX data for 2, 4, and 12-hour intervals were

obtained between October 15, 2020 (day 289 of 2020) and November 13, 2020 (day 318 of 2020), with the earthquake time as the reference. The obtained RINEX data were processes daily using the GAMIT/GLOBK scientific data evaluation software for all satellite combinations (MIX). The evaluation strategy included:

- IGS precise orbits (sp3),
- usno_bull_b orbit parameters,
- 14 IGS stations,
- Reference Frame: ITRF 2014,
- Ocean Loading Effect: FES2004,
- Zenith Delay: PWL (piecewise linear),
- Dry/Wet Troposphere: VMF1 (Vienna Mapping Function 1),
- Precursory Tropospheric Model: Global Pressure Temperature Model (GPT 50).

A total of 90 evaluations were performed, each evaluation varying between approximately 20 minutes and 60 minutes depending on the measurement duration (Gündoğan, 2023).

To investigate the earthquake's impact on point positioning, the average coordinate values before and after the earthquake were calculated for two different time periods: pre-earthquake and post-earthquake. The average errors of these values were also computed. Errors were calculated using the following parameters:

$$vx_{ö/s_i} = x_{ö/s_i} - x_{ort_{ö/s}} \quad vy_{ö/s_i} = y_{ö/s_i} - y_{ort_{ö/s}} \quad vh_{ö/s_i} = h_{ö/s_i} - h_{ort_{ö/s}} \tag{1}$$

The calculations were obtained using the equation for errors. In the equation, the subscript ö/s "pre/post" represents pre-earthquake and post-earthquake, "i" represents the order of measurement, and "$ort_{ö/s}$ " represents the pre-earthquake and post-earthquake averages. After obtaining the errors, the root mean square errors (m_x, m_y, m_h) were calculated using;

$$m_{x_{ö/s}} = \pm\sqrt{\frac{\left[\underset{\bar{s}_i}{vx_{ö}}\ \underset{\bar{s}_i}{vx_{ö}}\right]}{(n-1)}} \quad m_{y_{ö/s}} = \pm\sqrt{\frac{\left[vy_{ö/s_i}vy_{ö/s_i}\right]}{(n-1)}} \quad m_{h_{ö/s}} = \pm\sqrt{\frac{\left[vh_{ö/s_i}vh_{ö/s_i}\right]}{(n-1)}} \tag{2}$$

In the calculations, since data for 15 days before and after the earthquake were evaluated, "n" was taken as 15 in the equation. The differences between the average coordinate values calculated before and after the earthquake were calculated using;

$$dx = x_{ort_{ö}} - x_{ort_s} \quad dy = y_{ort_{ö}} - y_{ort_s} \quad dh = h_{ort_{ö}} - h_{ort_s} \tag{3}$$

The equation for the average error of the difference components was used in calculating the average error:

$$m_{d_x} = \pm\sqrt{m_{x_{ö}}^2 + m_{x_s}^2} \quad m_{d_y} = \pm\sqrt{m_{y_{ö}}^2 + m_{y_s}^2} \quad m_{d_h} = \pm\sqrt{m_{h_{ö}}^2 + m_{h_s}^2} \tag{4}$$

For each component, the test value was calculated using;

$$t_x = \frac{|dx|}{m_{d_x}} \quad t_y = \frac{|dy|}{m_{d_y}} \quad t_h = \frac{|dh|}{m_{d_h}} \tag{5}$$

The calculated test values were compared with the table value $\left(t_{table} = t_{f_1+f_2,1-\alpha} = t_{28,0.95} = 1.701\right)$ obtained from the t-distribution table. If the test value for even one component of a point was greater than the table value, it was determined that the point had displaced significantly. In determining the table value, f_1 represents the degrees of freedom before the earthquake, f_2 represents the degrees of freedom after the earthquake, and α represents the significance level (0.05).

3. RESULTS AND DISCUSSION

The comparison results of the t-distribution are provided in Tables 1-3.

Table 1. Statistical Information for 2-Hour Measurements

Stations ID	Coordinate differences (mm)		rmse of coordinates differences (mm)	Test Value	Comparison	Result
AKHI	dy	**13.4***	±2.1	6.500	$t_y > t_{tablo}$	Unstable
	dx	1.2	±1.2	1.000	$\boldsymbol{t_x < t_{tablo}}$	
	dh	**23.7***	±3.1	7.780	$t_h > t_{tablo}$	
BOZU	dy	6.2	±2.6	2.410	$t_y > t_{tablo}$	Unstable
	dx	12.0	±1.0	12.720	$t_x > t_{tablo}$	
	dh	8.7	±3.3	2.620	$t_h > t_{tablo}$	
CINC	dy	5.4	±2.6	2.090	$t_y > t_{tablo}$	Unstable
	dx	11.8	±1.1	10.890	$t_x > t_{tablo}$	
	dh	14.2	±4.1	3.470	$t_h > t_{tablo}$	
ESME	dy	9.1	±2.3	3.940	$t_y > t_{tablo}$	Unstable
	dx	3.8	±1.0	3.760	$t_x > t_{tablo}$	
	dh	6.1	±3.9	1.570	$\boldsymbol{t_h < t_{tablo}}$	
MNTS	dy	0.1	±2.5	0.040	$\boldsymbol{t_y < t_{tablo}}$	Unstable
	dx	**39.1***	±0.9	45.550	$t_x > t_{tablo}$	
	dh	22.0	±3.6	6.100	$t_h > t_{tablo}$	
SHUT	dy	4.7	±2.6	1.840	$t_y > t_{tablo}$	Unstable
	dx	6.8	±1.0	6.990	$t_x > t_{tablo}$	
	dh	3.8	±4.0	0.970	$\boldsymbol{t_h < t_{tablo}}$	
TVAS	dy	6.7	±2.8	2.370	$t_y > t_{tablo}$	Unstable
	dx	10.7	±1.0	10.410	$t_x > t_{tablo}$	
	dh	6.6	±4.3	1.520	$\boldsymbol{t_h < t_{tablo}}$	

As a result of the evaluation of the 2-hour measurements, it is observed that the maximum coordinate differences are at the AKHI station with 13.39 mm in the y-axis direction, at the MNTS station with 39.05 mm in the x-axis direction, at the AKHI station with 23.70 mm in the h-direction (vertical).

Table 2. Statistical Information for 4-Hour Measurements

Stations ID	Coordinate differences (mm)		rmse of coordinates differences (mm)	Test Value	Comparison	Result
AKHI	dy	0.9	±0.3	3.080	$t_y > t_{table}$	Unstable
	dx	2.0	±0.7	3.050	$t_x > t_{table}$	
	dh	0.1	±1.6	0.050	$\boldsymbol{t_h < t_{table}}$	
BOZU	dy	0.8	±0.2	4.500	$t_y > t_{table}$	Unstable
	dx	0.1	±0.3	0.440	$t_x < t_{table}$	
	dh	0.6	±1.0	0.630	$t_h < t_{table}$	
CINC	dy	0.4	±0.2	1.530	$\boldsymbol{t_y < t_{table}}$	Unstable
	dx	0.9	±0.2	3.540	$t_x > t_{table}$	
	dh	2.3	±1.3	1.720	$t_h > t_{table}$	
ESME	dy	2.0	±0.3	8.070	$t_y > t_{table}$	Unstable
	dx	1.0	±0.4	2.460	$t_x > t_{table}$	
	dh	**12.7***	±1.8	7.180	$t_h > t_{table}$	
MNTS	dy	**6.8***	±0.3	26.400	$t_y > t_{table}$	Unstable
	dx	**47.7***	±0.3	186.930	$t_x > t_{table}$	
	dh	7.9	±1.0	8.240	$t_h > t_{table}$	
SHUT	dy	0.3	±0.2	1.050	$\boldsymbol{t_y < t_{table}}$	Unstable
	dx	1.2	±0.2	6.400	$t_x > t_{table}$	
	dh	6.2	±0.8	8.190	$t_h > t_{table}$	
TVAS	dy	0.9	±0.4	2.220	$t_y > t_{table}$	Unstable
	dx	1.4	±0.3	4.760	$t_x > t_{table}$	
	dh	0.7	±1.0	0.680	$\boldsymbol{t_h < t_{table}}$	

As a result of the evaluation of the 4-hour measurements, it is observed that the maximum coordinate differences are at the MNTS station with 6.84 mm in the y-axis direction, at the MNTS station with 47.71 mm in the x-axis direction, at the ESME station with 12.70 mm in the h-direction (vertical).

Table 3. Statistical Information for 12-Hour Measurements

Stations ID	Coordinate differences (mm)		rmse of coordinates differences (mm)	Test Value	Comparison	Result
AKHI	dy	3.3	±0.2	20.080	$t_y > t_{table}$	Unstable
	dx	5.0	±0.2	20.380	$t_x > t_{table}$	
	dh	**3.4***	±0.6	6.000	$t_h > t_{table}$	
BOZU	dy	0.6	±0.1	4.440	$t_y > t_{table}$	Unstable
	dx	0.2	±0.2	1.370	$\boldsymbol{t_x < t_{table}}$	
	dh	0.9	±0.4	2.060	$t_h > t_{table}$	
CINC	dy	0.8	±0.1	5.320	$t_y > t_{table}$	Unstable
	dx	0.8	±0.1	7.600	$t_x > t_{table}$	
	dh	2.5	±0.4	5.840	$t_h > t_{table}$	
ESME	dy	1.5	±0.2	8.610	$t_y > t_{table}$	Unstable
	dx	0.8	±0.1	5.700	$t_x > t_{table}$	
	dh	0.3	±0.5	0.660	$\boldsymbol{t_h < t_{table}}$	
MNTS	dy	**7.0***	±0.2	43.660	$t_y > t_{table}$	Unstable
	dx	**48.0***	±0.1	376.420	$t_x > t_{table}$	
	dh	3.0	±0.4	7.120	$t_h > t_{table}$	
SHUT	dy	1.5	±0.2	7.790	$t_y > t_{table}$	Unstable
	dx	0.4	±0.2	2.380	$t_x > t_{table}$	
	dh	2.7	±0.6	4.760	$t_h > t_{table}$	
TVAS	dy	0.5	±0.2	2.100	$t_y > t_{table}$	Unstable
	dx	1.0	±0.1	7.160	$t_x > t_{table}$	
	dh	2.5	±0.7	3.750	$t_h > t_{table}$	

As a result of the evaluation of the 12-hour measurements, it is observed that the maximum coordinate differences are at the MNTS station with 6.96 mm in the y-axis direction, at the MNTS station with 48.01 mm in the x-axis direction and at the AKHI station with 3.40 mm in the h-direction (vertical).

The daily coordinate data from the stations were evaluated with time series analysis. As a result of these evaluations, a total of 21 graphs were plotted using GMT (The Generic Mapping Tools) for all stations. Since the station with the most significant change is MNTS, a graph from this station is provided as an example (Figure 3-5). In the graphs, the points in the middle of the vertical lines represent the station's location, and the length of the line represents the confidence interval.

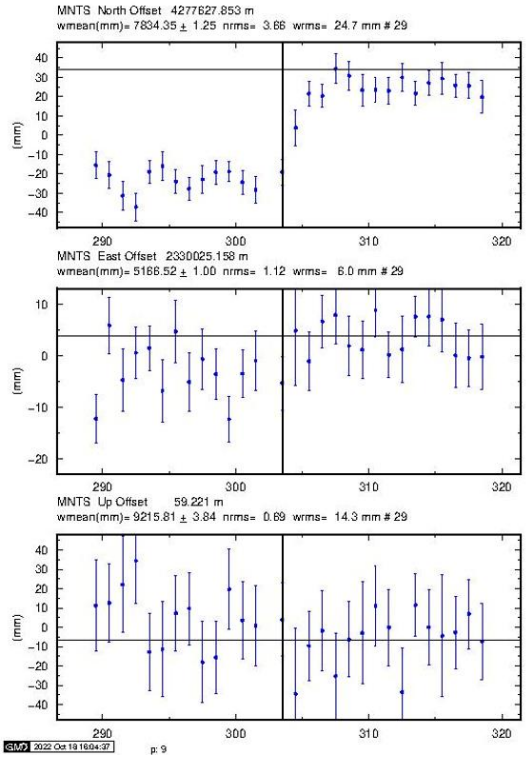

Figure 3. Time Series Analysis of Data from the MNTS Station with 2-Hour MIX Measurements

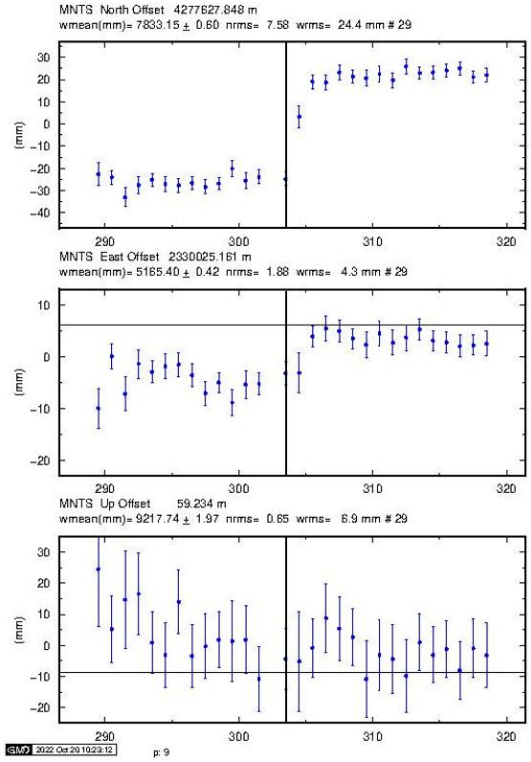

Figure 4. Time Series Analysis of Data from the MNTS Station with 4-Hour MIX Measurements

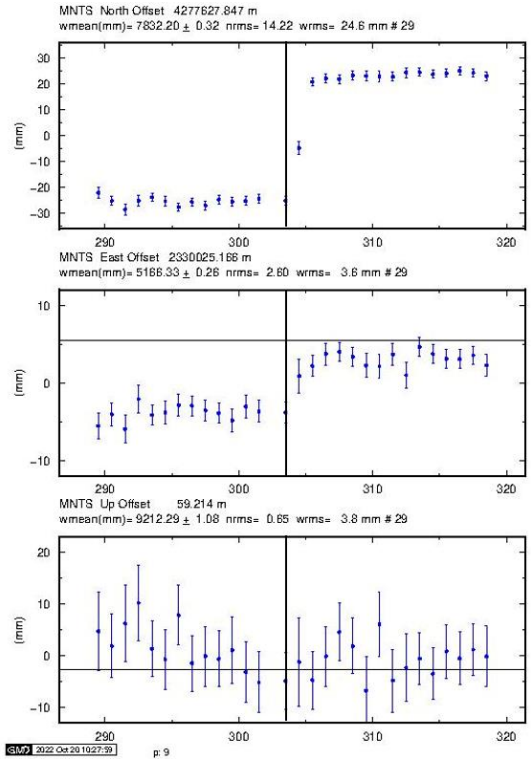

Figure 5. Time Series Analysis of Data from the MNTS Station with 12-Hour MIX Measurements

When examining Figures 3-5, it can be observed that as the measurement duration increases, the reliability of the measurements improves, and the changes at the points are better represented with 12-hour measurements.

4. CONCLUSIONS

In this study, the impact of the Aegean Sea Earthquake on TUSAGA stations was investigated. For this purpose, 7 stations located in the earthquake zone were used. The distances of these points to the earthquake center vary between ~60 and ~400 km. The stations considered for evaluation are AKHI, BOZU, CINC, ESME, MNTS, SHUT, and TVAS. The GNSS data for the GPS+GLONASS+Galileo combination at these stations were divided into groups of 2, 4, and 12 hours, considering 15 days before the earthquake, the earthquake day, and 15 days after the earthquake, with the earthquake hour as the reference point. The data were evaluated using 14 IGS stations in the GAMIT/GLOBK software. The coordinates before and after the earthquake in the selected stations were determined, and whether the differences between them are significant was investigated through statistical tests, with the results shown in Tables 1-3.

When examining Tables 1-3, it can be observed that as the measurement duration increases, the accuracy of coordinate differences improves. The best results were obtained with 12-hour measurements, and the largest displacement occurred at the MNTS station, which is the closest to the earthquake center. Following MNTS, the stations with the largest displacements are AKHI, ESME, SHUT, TVAS, CINC, and BOZU. The largest displacements at MNTS were 6.96 mm in the y-axis direction and 48.01 mm in the x-axis direction. The largest vertical displacement occurred at the AKHI station, with 3.40 mm. As the measurement duration increases, the impact of the earthquake on point positions becomes more evident. This is confirmed by the analysis of the data from the MNTS station in Figure 5.

Declaration of Ethical Standards

As the authors of this study, we declare that all ethical standards have been complied with.

Credit Authorship Contribution Statement

Author contribution rates in this study as follows: Tunahan Gündoğan 40%, Sercan BÜLBÜL 30%, Cevat İnal 30%.

Declaration of Competing Interest

The authors declare no conflict of interest.

Acknowledgements

This study was produced based on the Master's Thesis titled "The Effect of the Galileo Satellite System on Point Positioning" prepared by Tunahan GÜNDOĞAN under the supervision of Prof. Dr. Cevat İNAL in the Department of Geomatics Engineering at Konya Technical University, Graduate School of Natural and Applied Sciences.

Data Availability

All data used for this study are available from the corresponding author upon reasonable request.

5. REFERENCES

[1] A. Kürçer, H. Elmacı, F. Savaş, Ö. Kayadibi, "30 Ekim 2020 Ege Denizi Depremi (Mw 6,9) üzerine bir değerlendirme," *MTA Doğal Kaynaklar ve Ekonomi Bülteni*, vol. 30, pp. 57–75, 2020.

[2] Y. Yılmaz, "Ege Bölgesinin Aktif Tektoniği," in *Batı Anadolu'nun Depremselliği Sempozyumu*, 2000, pp. 3–14.

[3] S. Yaprak, O. Yildirim, and C. Inal, "Determination of 2011 Van/Turkey earthquake (M = 7.2) effects from measurements of CORS-TR network," *Geomatics, Natural Hazards and Risk*, vol. 5, no. 2, pp. 132–144, 2014, doi: 10.1080/19475705.2013.789453.

[4] C. Satirapod, W. J. F. Simons, and C. Promthong, "Monitoring Deformation of Thai Geodetic Network due to the 2004 Sumatra-Andaman and 2005 Nias Earthquakes by GPS," *Journal of Surveying Engineering*, vol. 134, no. 3, pp. 83–88, 2008, doi: 10.1061/(ASCE)0733-9453(2008)134:3(83).

[5] G. Wang and T. Soler, "Using OPUS for Measuring Vertical Displacements in Houston, Texas," *Journal of Surveying Engineering*, vol. 139, no. 3, pp. 126–134, 2013, doi: 10.1061/(ASCE)SU.1943-5428.0000103.

[6] M. Li, W. Li, R. Fang, C. Shi, and Q. Zhao, "Real-time high-precision earthquake monitoring using single-frequency GPS receivers," *GPS Solutions*, vol. 19, no. 1, pp. 27–35, 2015, doi: 10.1007/s10291-013-0362-4.

[7] G. Wang, Y. Bao, Y. Cuddus, X. Jia, J. Serna, and Q. Jing, "A methodology to derive precise landslide displacement time series from continuous GPS observations in tectonically active and cold regions: a case study in Alaska," *Natural Hazards*, vol. 77, no. 3, pp. 1939–1961, 2015, doi: 10.1007/s11069-015-1684-z.

[8] A. Richter *et al.*, "Crustal deformation across the Southern Patagonian Icefield observed by GNSS," *Earth Planet Sci Lett*, vol. 452, pp. 206–215, 2016, doi: https://doi.org/10.1016/j.epsl.2016.07.042.

[9] E. Gunawan, S. Widiyantoro, Zulfakriza, I. Meilano, and C. Pratama, "Postseismic deformation following the 2 July 2013 Mw 6.1 Aceh, Indonesia, earthquake estimated using GPS data," *J Asian Earth Sci*, vol. 177, pp. 146–151, 2019, doi: https://doi.org/10.1016/j.jseaes.2019.03.020.

[10] F. Jouanne *et al.*, "Postseismic deformation following the April 25, 2015 Gorkha earthquake (Nepal): Afterslip versus viscous relaxation," *J Asian Earth Sci*, vol. 176, pp. 105–119, 2019, doi: https://doi.org/10.1016/j.jseaes.2019.02.009.

[11] D. Baysal, B. Aktuğ, and A. Koçyiğit, "GPS Nokta Koordinatlarındaki Zamana Bağlı Değişimlerin Analizi ve Yorumu: İzmir Bölgesinde Uygulama," *Harita Dergisi*, vol. 144, pp. 29–39, Jul. 2010.

[12] T. Gündoğan, "Galileo Uydu sisteminin Nokta Konumlamaya Etkisi," Graduate Education Institute, Konya, 2023.

[13] R. M. Parameswaran, R. Grapenthin, M. E. West, and A. Fozkos, "Interchangeable Use of GNSS and Seismic Data for Rapid Earthquake Characterization: 2021 Chignik, Alaska, Earthquake," *Seismological Research Letters*, vol. 94, no. 3, pp. 1367–1378, Mar. 2023, doi: 10.1785/0220220357.

[14] S. Baselga and J. Najder, "Automated detection of discontinuities in EUREF permanent GNSS network stations due to earthquake events," *Survey Review*, vol. 54, no. 386, pp. 420–428, 2022, doi: 10.1080/00396265.2021.1964230.

[15] S. A. Younes, "Study of crustal deformation in Egypt based on GNSS measurements," *Survey Review*, vol. 55, no. 391, pp. 338–349, Jul. 2023, doi: 10.1080/00396265.2022.2099690.

[16] H.-U. Kim and T.-S. Bae, "Monitoring of Possible Activities of Yangsan Fault Zone Using GNSS," *Applied Sciences*, vol. 13, no. 3, 2023, doi: 10.3390/app13031862.

[17] S. Joshi, S. Kannaujiya, and U. Joshi, "Analysis of GNSS Data for Earthquake Precursor Studies Using IONOLAB-TEC in the Himalayan Region," *Quaternary*, vol. 6, no. 2, 2023, doi: 10.3390/quat6020027.

[18] M. J. Fuchs, M. Rexer, and F. Schaider, "Detection and analysis of seismic induced GNSS station motion in a North American network following the 2017 Chiapas earthquake," *J Geodyn*, vol. 149, p. 101881, 2022, doi: https://doi.org/10.1016/j.jog.2021.101881.